# Use of High-Resolution Volumetric MR Spectroscopic Imaging in Assessing Treatment Response of Glioblastoma to an HDAC Inhibitor

Hyunsuk Shim, *Emory University*
Li Wei, *Emory University*
Andrew H Miller, *Emory University*
Jeffrey James Olson, *Emory University*
Chad A Holder, *Emory University*
Ying Guo, *Emory University*
Xiaoping P Hu, *Emory University*

## Copyright information:

# Use of High-Resolution Volumetric MR Spectroscopic Imaging in Assessing Treatment Response of Glioblastoma to an HDAC Inhibitor

**Hyunsuk Shim**[1,2], **Li Wei**[3], **Chad A. Holder**[1], **Ying Guo**[4], **Xiaoping P. Hu**[3], **Andrew H. Miller**[2,5], and **Jeffrey J. Olson**[2,6]

[1]Department of Radiology and Imaging Sciences, Emory University, 1701 Uppergate Dr, C5018, Atlanta, GA 30322

[2]Winship Cancer Institute, Emory University, Atlanta, GA

[3]Department of Biomedical Engineering, Emory University, Atlanta, GA

[4]Department of Biostatistics, Emory University, Atlanta, GA

[5]Department of Psychiatry, Emory University, Atlanta, GA

[6]Department of Neurosurgery, Emory University, Atlanta, GA

## Abstract

**Objective**—Improved predictive imaging would enable personalization and adjustment of treatment, which are critical for patients with glioblastomain whom therapy is likely to fail. This article describes the use of MR spectroscopic imaging (MRSI) to predict early clinical and behavioral response to a therapy and an effort to develop high-resolution, volumetric MRSI to improve its clinical application.

**Conclusion**—MRSI may enable quantitative analysis of brain tumor response, offering a precise tool for monitoring of patients in clinical trials.

## Keywords

epigenetic modification; glioblastoma; histone deacetylase (HDAC); MR spectroscopic imaging; vorinostat

Glioblastoma is the most common primary malignant brain tumor in adults. About 12,000 new cases are diagnosed each year in the United States [1]. The current standard of care is maximal safe resection (ideally, gross total resection) followed by radiation therapy with concurrent and adjuvant oral temozolomide chemotherapy. Surgical debulking of these tumors has been shown to improve patient outcome (quality of life and progression-free survival) but has inconsistently resulted in improved overall survival [2]. Although incremental progress has been made in the management of these tumors with the relatively

Address correspondence to H. Shim (hshim@emory.edu).
H. Shim and L. Wei contributed equally to this work.

recent addition of temozolomide to radiation therapy, outcomes remain poor, with a median survival of only 14.6 months [3, 4]. Currently, glioblastomas are typically imaged with conventional MRI sequences, which include T2-weighted, FLAIR, and unenhanced and contrast-enhanced T1-weighted sequences. Gross tumor shows heterogeneous enhancement on contrast-enhanced T1-weighted images, whereas surrounding areas of high signal intensity on T2-weighted and FLAIR images represent a combination of edema and tumor infiltration or nonenhancing tumor. Although conventional MRI cannot accurately distinguish edema from nonenhancing infiltrating tumor, it is generally thought that standard MRI is adequate for determining the volume at risk for failure at pretreatment because the great majority of tumor recurrences are within the high dose regions of treatment [5–7].

## Current Problems Using Standard-of-Care MRI to Monitor Response to Therapy in Glioblastoma Patients

Epigenetic silencing of the $O^6$-methylguanine-DNA methyltransferase gene promoter compromises DNA repair and has been associated with longer survival in patients with glioblastoma treated with temozolomide [8]. The addition of temozolomide to radiation therapy for glioblastomas has resulted in a higher incidence of pseudoprogression than previously occurred with radiation therapy alone, a phenomenon whereby increased contrast enhancement is seen in responding tumors within the first 3–6 months after completion of radiation therapy [9, 10]. Enhancing regions of pseudoprogression and early true progression are indistinguishable on contrast-enhanced T1-weighted images. Both exhibit increase in size or number of enhancing lesions on contrast-enhanced T1-weighted images with increased vascular permeability, edema, and mass effect. Accurate distinction is needed for appropriate clinical management to either continue effective treatment (in the case of pseudoprogression) or to stop unhelpful treatment and avoid unnecessary toxicity and cost and potentially enroll the patient in clinical trials (in the case of early true progression). Diffusion-weighted imaging (DWI)–derived apparent diffusion coefficient (ADC) has been proposed to serve as a tool to differentiate pseudoprogression from early true progression. DWI measures water diffusion, which is independent of contrast leakage, and shows restricted diffusion in hypercellular tumors (i.e., a lower ADC implies a higher cell density). Mean ADC is lower in true progression than in pseudoprogression with statistical significance; however, values from individual patients overlap significantly [11, 12]. Another popular advanced MRI technology is perfusion-weighted MRI (PWI). Relative cerebral blood volume measurements derived from PWI can be used to identify and quantify areas of neovascularity or neoangiogenesis. Young et al. [13] reported that relative CBV was statistically higher in true progression than in pseudoprogression. Again, however, the values from individual patients overlap. In addition, Song et al. [14] reported that normalized CBV was not statistically different between two groups.

Conversely, the use of antiangiogenic agents (e.g., bevacizumab or cediranib) has reportedly increased the incidence of pseudoresponse, complicating the interpretation of standard MR images [15]. These agents rapidly decrease the extent of contrast-enhancing tumor volume due to restoration of the blood-brain-barrier and leaky tumor vasculature, with almost no impact on overall survival [16]. This is often accompanied by an increase in the extent of

abnormal signal intensity on T2-weighted and FLAIR images as well as on diffusion-weighted images and ADC maps (nonenhancing tumor progression), suggesting that inhibition of angiogenesis may stimulate other mechanisms of tumor dissemination.

PET, an alternative imaging modality, complements MRI by providing the opportunity to assess physiologic and biochemical activity in normal tissues and to directly compare the functional activity in tumors to that of adjacent tissue. The most widely used PET agent for detecting brain and systemic tumors has been ^{18}F-FDG, which has also been used to assess radiation-induced tissue necrosis and response to treatment [17, 18]. Although FDG PET has been shown to be an effective tumor imaging agent, it has serious shortcomings because interpretation is often complicated by high glycolytic uptake by normal brain tissue and ischemic brain tissue.

## MRSI as Alternative Imaging

Proton MR spectroscopy (MRS) and MRS imaging (MRSI) can characterize regions of brain on the basis of mapping of various metabolites and other substances [19, 20]. Metabolites that can be evaluated include choline (Cho), which is nearly always elevated in non-necrotic areas of malignant gliomas; creatine (Cr), an energy metabolite that can serve as an internal control resonance; *N*-acetyl aspartate (NAA), which is a marker of viable neurons; and lactate (Lac), which is a product of anaerobic glycolysis, hypoxia, or ischemia, such as can be seen in hypoxic tumors. Early studies using MRS established that the spectra obtained from glioblastomas differ significantly from those obtained from normal brain, with increased levels of Cho and Lac, and decreased levels of NAA. Park et al. [21] correlated the pattern of recurrence after radiation therapy with MRSI findings. They noted that eight of nine patients with a growing enhancing lesion after radiation therapy had recurrence in regions that were defined by a combination of standard contrast-enhanced MRI and MRSI parameters (using a Cho-to-NAA ratio cutoff of two with TR/TE, 1000/144). In addition, Stadlbauer et al. [22–24] showed in gliomas that MRSI-derived Cho-to-NAA ratios frequently identified regions at higher risk of tumor beyond the T2-hyperintense signal abnormalities and concluded that MRSI may be useful for delineating nonenhancing portions of infiltrating tumors.

In practice, MRSI has not been used to its full potential in the clinical setting because of low spatial resolution, long acquisition times, and insufficient tools for image processing and display in current commercially available forms. In fact, the MRSI data are often of in-sufficient quality for clinical use with "out-of-the-box" vendor-provided sequences. Recent advances in MRSI technology and development of image registration and visualization tools that enable clinicians to assess and evaluate MRSI data more easily would help to clear these hurdles that have made routine clinical application difficult. Supported by a grant from the Bioengineering Research Partnership (BRP; R01EB000822), Sabati et al. [25] developed an advanced MRSI methodology combining 3D echo-planar spectroscopic imaging with parallel imaging. A short TE (17.6 ms) and high-spatial-resolution version of this sequence was recently installed on a 3-T research MRI scanner at Emory University. This enables acquisition of whole-brain 3D MRSI ($4.4 \times 4.4 \times 5.6$ mm nominal voxel size, 0.108 mL, or 108 μL) in 12 minutes. This acquisition method collects internal water signal intensity as a

denominator to obtain absolute metabolite concentrations in an interleaved manner without increasing total scanning time. A sample dataset from a healthy volunteer was analyzed using the Metabolic Imaging Data Analysis System (MIDAS) developed at the University of Miami [26]. Although MIDAS is an excellent program for processing complex MRSI data, it is not optimally user-friendly at this time nor does it enable busy clinicians to review and analyze the data in a 3D format easily. Velocity AI, an Emory-developed and licensed Food and Drug Administration 510k–approved software suite with robust deformable image coregistration capabilities [27], was then used to display an NAA metabolite map from a healthy subject (Fig. 1). The NAA map, which was fused with T1-weighted 3D magnetization-prepared rapid gradient-echo anatomic MR images, shows the varying levels of NAA throughout the brain. Figure 2 shows a Cho-to-NAA metabolite ratio map from a glioblastoma patient 2 weeks after resection of the tumor using Velocity AI. Although the residual enhancing tumor estimated by subtracting contrast-enhanced T1-weighted images from unenhanced T1-weighted images measured 1.1 mL (almost gross total resection), the Cho-to-NAA ratio map reveals more extensive residual infiltrating tumor with much greater sensitivity.

In addition to the volumetric 3D MRSI map, a desirable output of MRSI results requires quantitative analysis (average or maximum) of treatment-induced metabolic changes in spatially coregistered MRSI from individual selected voxels (or groups of voxels). Furthermore, this selection of voxels in discrete tumor and peritumoral regions on anatomic MR images should be performed by an automated or semiautomated method that is unbiased and capable of reproducible tumor segmentation using rigid or deformable image coregistration. This method will enable quantitative analysis of brain tumor response to chemotherapy, radiation, and surgical therapies, offering a precise tool for longitudinal monitoring of patients in clinical trials.

## Histone Deacetylase Inhibitor Combined With Standard-of-Care Treatment in Glioblastomas

In this article, we review a pilot clinical trial to evaluate an epigenetic drug, suberoylanilide hydroxamic acid (vorinostat, Zolinza, Merck) for the treatment of recurrent glioblastomas, using imaging to assess therapy response in the challenging setting of pseudoprogression. Epigenetic modifications are now recognized as a frequent occurrence in the early phases of tumorigenesis, playing a central role in tumor development. Epigenetic alterations differ significantly from genetic modifications in that they may be reversed by epigenetic drugs, such as histone deacetylase (HDAC) inhibitors. Vorinostat is an orally active, potent inhibitor of HDAC activity that crosses the blood-brain barrier. Among the pleiotropic effects of HDAC inhibitors is the ability to attenuate inflammation, an action seen at concentrations lower than those required to slow cancer cell growth [28, 29]. Glioblastoma is frequently associated with neuroinflammation, which is thought to have protumorigenic effects. Hypoxic and necrotic regions of glioblastomas are most highly associated with inflammatory cell infiltrates, and gene expression profiling reveals a signature associated with hypoxia-in-ducible genes involved in angiogenesis and inflammation [30]. Such changes are associated with recruitment of macrophages along a hypoxia-mediated

chemotactic gradient. Macrophages recruited to hypoxic sites exert tumor-promoting effects through the expression of genes with mitogenic, angiogenic, and migration-invasion stimulating properties [31]. Abrogating inflammatory changes associated with glioblastoma might reduce or eliminate access to these tumor-promoting effects.

### Antidepressant Effects of Histone Deacetylase Inhibitors

Another intriguing effect of HDAC inhibitors as anticancer agents is their mood-enhancing, potentially antidepressant, properties. In mice, increased histone acetylation in key mood-relevant genes was found after chronic social defeat stress, a mouse model of depression [32]. Similar findings were observed in depressed humans on postmortem examinations. Moreover, infusion of HDAC inhibitors into the brain of mice exposed to chronic social defeat exerted potent antidepressant effects. These findings are especially relevant given the high frequency of depression (15– 39%) in patients with brain tumor [33]. In this patient population, depression is consistently associated with cognitive impairment, reduced physical function, and poor quality of life. The antidepressant effects of HDAC inhibitors may be due to their antiinflammatory properties given recent data implicating inflammation in the development of depression, including the identification of activated microglia in postmortem brains of depressed individuals [32, 34]. As noted, glioblastomas are infiltrated with inflammatory cells, including macrophages. Although the presence of inflammatory cells in glioblastomas and the incidence of clinical depression in patients with glioblastomas have not been correlated, these findings are suggestive and worth exploring.

### MRSI Biomarkers for Therapy Monitoring

Based on these observations, patients with glioblastoma could benefit from therapy with HDAC inhibitors, such as vorinostat. Response to vorinostat therapy is associated with tumor redifferentiation and cytostasis rather than outright tumor size reduction on standard MRI, further limiting the use of traditional MRI methods for evaluation of treatment response. A noninvasive method to assess drug delivery and impact on the tumor was needed. Spectra from glioblastomas differ from normal brain spectra, with increased levels of Cho and Lac and decreased levels of NAA [35, 36]. Another important compound is myoinositol, a carbocyclic polyol that is the precursor of a number of secondary messengers in eukaryotic cells, including inositol phosphate lipid derivatives. Myoinositol is synthesized from glucose-6-phosphate in two steps: glucose-6-phosphate is isomerized by inositol-3-phosphate synthase (*ISYNA1* or myoinositol phosphate) to inositol-1-phosphate and inositol-1-phosphate is dephosphorylated by inositol monophosphatase 1 to give free myoinositol [37, 38]. In addition to decreased myoinositol in cancer cells, the CSF of noncancer patients with depression shows low myoinositol levels, and treating these patients with myoinositol significantly improves depressive symptoms [39, 40]. The HDAC *RPD3* can directly regulate myoinositol phosphate and affect cellular myoinositol levels in yeast [41], suggesting that vorinostat may also affect myoinositol metabolism, potentially reversing changes associated with malignancy and depression. Elevation of myoinositol is also known to be associated with low-grade glial neoplasms, whereas it is decreased in high-grade gliomas [39]. Collectively, these data suggest that myoinositol could be a biomarker to quantify response to vorinostat therapy associated with redifferentiation. A preclinical study [42] showed that normalization or restoration of $^1$H MRS metabolites could be reliable

imaging biomarkers for an early favorable response to vorinostat treatment in an orthotopic animal model for glioma and that reduction in myoinositol and NAA was found to be a potential biomarker for depression, which may also be alleviated with vorinostat treatment.

## A Case Report

In March 2011, we opened an Emory investigator-initiated trial to treat glioblastoma patients with vorinostat and temozolomide after progression on standard-of-care radiation therapy and temozolomide or new experimental antiangiogenic therapy. To assess whether MRS predicts a biologic and possibly redifferentiating effect of vorinostat, we adapted and optimized 2D chemical-shift imaging (CSI). This trial occurred before high-resolution volumetric MRSI was available. The subjects received a regimen of vorinostat 400 mg by mouth daily for 1 week. Baseline MRS was performed 1–3 days before initiation of treatment. Follow-up MRS studies were performed at day 7 and at week 9. A standard quadrature head coil was used to collect MR data. Two-dimensional CSI was performed using a stimulated-echo acquisition mode sequence on a 3-T research scanner (Tim Trio, Siemens Healthcare): TR/TE, 1590/30; matrix, $16 \times 16$; FOV, $180 \times 180$ mm; acquisition time, 10 minutes). All CSI data were analyzed by LC model software (open source, using an 18-metabolite basis set and the intracellular water signal as the internal reference. The change of metabolite level ($\Delta Met$) was calculated in ratio by ($Met_{after\ treatment}/Met_{before\ treatment} - 1$). The spectroscopic restoration index was calculated ($\Delta NAA + \Delta CR + \Delta MI - \Delta Cho - \Delta (lac/lipids)$) and used to classify responders and nonresponders. In addition, we assessed levels of depression using the Inventory of Depressive Symptoms–Self Report (IDS-SR) [43] to determine whether metabolite changes were associated with changes in severity of depressive symptoms. Higher IDS-SR scores reflect greater severity of depression. Figure 3 shows an example of the metabolite maps generated from data acquired from a glioblastoma patient who had been treated by vorinostat for 7 days followed by vorinostat combined with temozolomide for 8 more weeks. Before treatment, the left frontoparietal glioblastoma showed decreased levels of NAA (suggesting neuronal destruction or displacement), Cr, and myoinositol as well as elevated Lac (suggesting increased anaerobic glycolysis in hypoxic regions resulting from rapid tumor growth). After 7 days of vorinostat therapy, levels of NAA, myoinositol, and Cr increased around the rim of the tumor by 0.18, 0.25, and 0.32, respectively, and Cho and Lac decreased by 0.14 and 0.52, respectively, representing a move toward normalization of these metabolites and possibly suggesting early cellular differentiation. The spectroscopic restoration index, the summation of the fractional changes in these five metabolites, was 1.40 [44, 45]. In many glioblastomas, viable cells are around the rim (margin) of the tumor, with mostly nonviable necrosis centrally. IDS-SR depression scores for this patient decreased (improved) by eight points after 7 days of vorinostat treatment. At the completion of the treatment (9 weeks of vorinostat and temozolomide), NAA, myoinositol, and Cr further increased and Lac decreased, supporting continued vorinostat efficacy as a differentiation-inducing agent in this patient. Contrast-enhanced T1-weighted MRI and perfusion studies at 9 weeks were concordant with the MRSI data, showing a good response to vorinostat treatment.

Another glioblastoma patient treated with vorinostat showed a different MRSI pattern than the previous patient. After 7 days of vorinostat treatment, no changes that would be

anticipated from a responder were seen. In particular, myoinositol was not improved. In addition, the IDS-SR score worsened (increased nine points) after 7 days of vorinostat. Even after 9 weeks of vorinostat and temozolomide treatment, MRSI did not show restoration of normal levels of metabolites. MRI showed a 19% increase in enhancing tumor volume with no change in perfusion on the relative CBV map [44].

Figure 3C summarizes the spectroscopic restoration index values and changes in the IDS-SR results and the Cho-to-NAA ratio of the first seven patients with usable data who were enrolled into our R21 Quick Trial. Patients who completed our study are listed by patient registry number. There was a clear separation in the spectroscopic restoration index values that appeared as good, if not better than, changes in the Cho-to-NAA ratio between the three metabolic responders and the three metabolic non-responders. Two-sided Student $t$ tests were used to compare the spectroscopic restoration index between metabolic responders and metabolic nonresponders. There was a highly significant difference between the spectroscopic restoration index values of the two groups ($p < 0.001$). Of note, the response rate based on contrast-enhanced MRI, defned by 25% increase in sum of the products of perpendicular diameters of enhancing lesions over baseline, was only 16%, whereas that on the spectroscopic restoration index was 43%. Further studies are needed to determine whether metabolic responders are indeed true responders in more homogeneous patient populations, e.g., new glioblastoma patients using overall survival rather than progression-free survival on contrast-enhancing T1-weighted MRI. Of note, IDS-SR depression scores for the three metabolic responders significantly decreased (improved) after 7 days of vorinostat treatment ($p = 0.03$), whereas those for metabolic nonresponders showed no significant change ($p = 0.30$). In addition, repeated measures ANOVA showed a significant difference in the IDS-SR scores, changing pattern from baseline to 7 days of vorinostat treatment between the metabolic responders and nonre-sponders ($p = 0.05$), with metabolic responders exhibiting greater decreases (improvement) in IDS-SR scores than metabolic nonresponders. Finally, there was a trend for a negative correlation between spectroscopic restoration index and IDS-SR scores (Spearman $\rho$, –0.70; $p = 0.07$), with higher spectroscopic restoration index scores associated with lower depressive symptoms in this small sample.

## Inconsistency Between MRI and MRSI

After only 7 days of vorinostat treatment, MRSI can distinguish metabolic responders (normalization or restoration of tumor metabolites toward normal brainlike metabolism) from nonresponders (no significant change in tumor metabolite profile). Our initial cohort ($n = 7$) consisted of three responders and four nonresponders with highly significant differences in their change in metabolite levels ($p < 0.001$). In the case of patient 002, although spectroscopic restoration index and IDS-SR results strongly suggested that the tumor responded to vorinostat treatment, the standard-of-care MRI (contrast-enhanced T1-weighted) showed increase in enhancement during the bevacizumab rebound period (the patient enrolled in our study 2 weeks after stopping bevacizumab antiangiogenic treatment). Therefore, by standard definitions, this patient was classified as a clinical nonresponder. Patient 008 enrolled in our trial showing metabolic responder MRSI results. This patient was enrolled in our study at 3 months after radiotherapy and temozolomide treatment because

contrast-enhanced T1-weighted MRI showed an increase in size of the area of enhancement. Although MRSI data showed this patient to be a metabolic responder, she was withdrawn from our trial at week 5 because of the worsening contrast-enhanced T1-weighted MRI. One week later, the enhancing lesion was biopsied and pathology assessment with H and E stains confirmed a combination of well-differentiated tumor (which appeared of lower grade than the original tumor histopathology) and necrotic tissue (Fig. 4). In addition, immunohistochemistry of acetylated histone H4 (marker for HDAC inhibitor response) showed that the tumor responded well to vorinostat treatment.

Our results provide exciting insights into the mechanisms by which HDAC inhibitors exert their effect on glioblastomas. Tumor cells have increased biosynthetic needs requiring reprogramming of cellular metabolism. This creates increased energy demands, making tumor cells even more vulnerable to interventions targeting their metabolism. HDAC inhibitors may induce redifferentiation in tumors by targeting tumor metabolism. Thus, the changes measured by MRSI may serve as reliable early predictors of response to HDAC inhibitor–containing combination therapies in glioblastomas.

## Conclusion

Drugs working by an epigenetic mechanism, such as vorinostat, can be a critical component of the cocktail of drugs for glioblastoma patients because 35–40% of glioblastomas have epigenetic modifications as the underlying mechanism driving malignancy. As opposed to contrast-enhanced T1-weighted anatomic MRI, MRSI highlights tumor cells on the basis of their altered metabolism and may provide greater accuracy for localizing metabolically active tumor extent and margins. Identification of a metabolite signature that shows significant tumor cell infiltration into normal brain in regions that do not appear abnormal on standard MRI would be of great value to neurosurgeons, radiation oncologists, and neurooncologists in optimizing brain tumor treatment. Combining high-resolution 3D volumetric MRSI with a sophisticated image coregistration platform will transform MRSI into a practical clinical tool for predicting clinical and behavioral responses and helping guide the care of patients with brain tumor.

## Acknowledgments

## References

1. Dolecek TA, Propp JM, Stroup NE, Kruchko C. CBTRUS statistical report: primary brain and central nervous system tumors diagnosed in the United States in 2005–2009. Neuro Oncol. 2012; 14(suppl 5):v1–v49. Erratum in Neuro Oncol 2013 May;15:646–647. [PubMed: 23095881]

2. Vuorinen V, Hinkka S, Farkkila M, Jaaskelainen J. Debulking or biopsy of malignant glioma in elderly people: a randomised study. Acta Neurochir (Wien). 2003; 145:5–10. [PubMed: 12545256]

3. Stupp R, Hegi ME, Mason WP, et al. Effects of radiotherapy with concomitant and adjuvant temozolomide versus radiotherapy alone on survival in glioblastoma in a randomised phase III study: 5-year analysis of the EORTC-NCIC trial. Lancet Oncol. 2009; 10:459–466. [PubMed: 19269895]

4. Stupp R, Mason WP, van den Bent MJ, et al. Radiotherapy plus concomitant and adjuvant temozolomide for glioblastoma. N Engl J Med. 2005; 352:987–996. [PubMed: 15758009]

5. Chan JL, Lee SW, Fraass BA, et al. Survival and failure patterns of high-grade gliomas after three-dimensional conformal radiotherapy. J Clin Oncol. 2002; 20:1635–1642. [PubMed: 11896114]

6. Lee SW, Fraass BA, Marsh LH, et al. Patterns of failure following high-dose 3-D conformal radiotherapy for high-grade astrocytomas: a quantitative dosimetric study. Int J Radiat Oncol Biol Phys. 1999; 43:79–88. [PubMed: 9989517]

7. Wallner KE, Galicich JH, Krol G, Arbit E, Malkin MG. Patterns of failure following treatment for glioblastoma multiforme and anaplastic astrocytoma. Int J Radiat Oncol Biol Phys. 1989; 16:1405–1409. [PubMed: 2542195]

8. Hegi ME, Diserens AC, Gorlia T, et al. *MGMT* gene silencing and benefit from temozolomide in glioblastoma. N Engl J Med. 2005; 352:997–1003. [PubMed: 15758010]

9. Brandes AA, Franceschi E, Tosoni A, et al. *MGMT* promoter methylation status can predict the incidence and outcome of pseudoprogression after concomitant radiochemotherapy in newly diagnosed glioblastoma patients. J Clin Oncol. 2008; 26:2192–2197. [PubMed: 18445844]

10. Brandsma D, van den Bent MJ. Pseudoprogression and pseudoresponse in the treatment of gliomas. Curr Opin Neurol. 2009; 22:633–638. [PubMed: 19770760]

11. Chu HH, Choi SH, Ryoo I, et al. Differentiation of true progression from pseudoprogression in glioblastoma treated with radiation therapy and concomitant temozolomide: comparison study of standard and high-b-value diffusion-weighted imaging. Radiology. 2013; 269:381–340.

12. Lee WJ, Choi SH, Park CK, et al. Diffusion-weighted MR imaging for the differentiation of true progression from pseudoprogression following concomitant radiotherapy with temozolomide in patients with newly diagnosed high-grade gliomas. Acad Radiol. 2012; 19:1353–1361. [PubMed: 22884399]

13. Young RJ, Gupta A, Shah AD, et al. MRI perfusion in determining pseudoprogression in patients with glioblastoma. Clin Imaging. 2013; 37:41–49. [PubMed: 23151413]

14. Song YS, Choi SH, Park CK, et al. True progression versus pseudoprogression in the treatment of glioblastomas: a comparison study of normalized cerebral blood volume and apparent diffusion coefficient by histogram analysis. Korean J Radiol. 2013; 14:662–672. [PubMed: 23901325]

15. Hygino da Cruz LC Jr, Rodriguez I, Domingues RC, Gasparetto EL, Sorensen AG. Pseudoprogression and pseudoresponse: imaging challenges in the assessment of posttreatment glioma. AJNR. 2011; 32:1978–1985. [PubMed: 21393407]

16. Batchelor TT, Sorensen AG, di Tomaso E, et al. AZD2171, a pan-VEGF receptor tyrosine kinase inhibitor, normalizes tumor vasculature and alleviates edema in glioblastoma patients. Cancer Cell. 2007; 11:83–95. [PubMed: 17222792]

17. Alavi JB, Alavi A, Chawluk J, et al. Positron emission tomography in patients with glioma: a predictor of prognosis. Cancer. 1988; 62:1074–1078. [PubMed: 3261622]

18. Tralins KS, Douglas JG, Stelzer KJ, et al. Volumetric analysis of $^{18}$F-FDG PET in glioblastoma multiforme: prognostic information and possible role in definition of target volumes in radiation dose escalation. J Nucl Med. 2002; 43:1667–1673. [PubMed: 12468518]

19. Go KG, Keuter EJ, Kamman RL, et al. Contribution of magnetic resonance spectroscopic imaging and L- [1-$^{11}$C]tyrosine positron emission tomography to localization of cerebral gliomas for biopsy. Neurosurgery. 1994; 34:994–1002. discussion, 1002. [PubMed: 8084410]

20. Negendank WG, Sauter R, Brown TR, et al. Proton magnetic resonance spectroscopy in patients with glial tumors: a multicenter study. J Neurosurg. 1996; 84:449–458. [PubMed: 8609557]

21. Park I, Tamai G, Lee MC, et al. Patterns of recurrence analysis in newly diagnosed glioblastoma multiforme after three-dimensional conformal radiation therapy with respect to pre-radiation therapy magnetic resonance spectroscopic findings. Int J Radiat Oncol Biol Phys. 2007; 69:381–389. [PubMed: 17513061]

22. Stadlbauer A, Buchfelder M, Doelken MT, Hammen T, Ganslandt O. Magnetic resonance spectroscopic imaging for visualization of the infiltration zone of glioma. Cent Eur Neurosurg. 2011; 72:63–69. [PubMed: 20635312]

23. Stadlbauer A, Moser E, Gruber S, et al. Improved delineation of brain tumors: an automated method for segmentation based on pathologic changes of ^{1}H-MRSI metabolites in gliomas. Neuroimage. 2004; 23:454–461. [PubMed: 15488395]

24. Stadlbauer A, Nimsky C, Buslei R, et al. Proton magnetic resonance spectroscopic imaging in the border zone of gliomas: correlation of metabolic and histological changes at low tumor infiltration — initial results. Invest Radiol. 2007; 42:218–223. [PubMed: 17351427]

25. Sabati M, Zhan J, Govind V, Arheart KL, Maudsley AA. Impact of reduced k-space acquisition on pathologic detectability for volumetric MR spectroscopic imaging. J Magn Reson Imaging. 2014; 39:224–234. [PubMed: 23559504]

26. Maudsley AA, Darkazanli A, Alger JR, et al. Comprehensive processing, display and analysis for in vivo MR spectroscopic imaging. NMR Biomed. 2006; 19:492–503. [PubMed: 16763967]

27. Kirby N, Chuang C, Ueda U, Pouliot J. The need for application-based adaptation of deformable image registration. Med Phys. 2013; 40:011702. [PubMed: 23298072]

28. Sigalotti L, Fratta E, Coral S, et al. Epigenetic drugs as pleiotropic agents in cancer treatment: biomolecular aspects and clinical applications. J Cell Physiol. 2007; 212:330–344. [PubMed: 17458893]

29. Dinarello CA, Fossati G, Mascagni P. Histone deacetylase inhibitors for treating a spectrum of diseases not related to cancer. Mol Med. 2011; 17:333–352. [PubMed: 21556484]

30. Du R, Lu KV, Petritsch C, et al. HIF1alpha induces the recruitment of bone marrow-derived vascular modulatory cells to regulate tumor angiogenesis and invasion. Cancer Cell. 2008; 13:206–220. [PubMed: 18328425]

31. Lewis CE, Pollard JW. Distinct role of macrophages in different tumor microenvironments. Cancer Res. 2006; 66:605–612. [PubMed: 16423985]

32. Covington HE 3rd, Maze I, LaPlant QC, et al. Antidepressant actions of histone deacetylase inhibitors. J Neurosci. 2009; 29:11451–11460. [PubMed: 19759294]

33. Rooney AG, Carson A, Grant R. Depression in cerebral glioma patients: a systematic review of observational studies. J Natl Cancer Inst. 2011; 103:61–76. [PubMed: 21106962]

34. Miller AH, Maletic V, Raison CL. Inflammation and its discontents: the role of cytokines in the pathophysiology of major depression. Biol Psychiatry. 2009; 65:732–741. [PubMed: 19150053]

35. Kugel H, Heindel W, Ernestus RI, Bunke J, du Mesnil R, Friedmann G. Human brain tumors: spectral patterns detected with localized H-1 MR spectroscopy. Radiology. 1992; 183:701–709. [PubMed: 1584924]

36. Ott D, Hennig J, Ernst T. Human brain tumors: assessment with in vivo proton MR spectroscopy. Radiology. 1993; 186:745–752. [PubMed: 8430183]

37. Nelson, DL.; Cox, MM. Lehninger principles of biochemistry. 4th. New York, NY: W. H. Freeman; 2005.

38. Salway, JG. Metabolism at a glance. 3rd. Malden, MA: Blackwell; 2004.

39. Castillo M, Smith JK, Kwock L. Correlation of myo-inositol levels and grading of cerebral astrocytomas. AJNR. 2000; 21:1645–1649. [PubMed: 11039343]

40. Hattingen E, Raab P, Franz K, Zanella FE, Lanfermann H, Pilatus U. Myo-inositol: a marker of reactive astrogliosis in glial tumors? NMR Biomed. 2008; 21:233–241. [PubMed: 17562554]

41. Rundlett SE, Carmen AA, Suka N, Turner BM, Grunstein M. Transcriptional repression by UME6 involves deacetylation of lysine 5 of histone H4 by RPD3. Nature. 1998; 392:831–835. [PubMed: 9572144]

42. Wei L, Hong S, Yoon Y, et al. Early prediction of response to vorinostat in an orthotopic glioma rat model. NMR Biomed. 2012; 25:1104–1111. [PubMed: 22302519]

43. Rush AJ, Giles DE, Schlesser MA, Fulton CL, Weissenburger J, Burns C. The Inventory for Depressive Symptomatology (IDS): preliminary findings. Psychiatry Res. 1986; 18:65–87. [PubMed: 3737788]

44. Shim, H.; Voloschin, A.; Wei, L., et al. American Society of Clinical Oncology (ASCO) Annual Meeting. Chicago, IL: ASCO; 2012. Using proton MRS to predict response to vorinostat treatment in recurrent GBM.

45. Shim H, Holder CA, Olson JJ. Magnetic resonance spectroscopic imaging in the era of pseudoprogression and pseudoresponse in glioblastoma patient management. CNS Oncology. 2013; 2:393–396. [PubMed: 25054660]
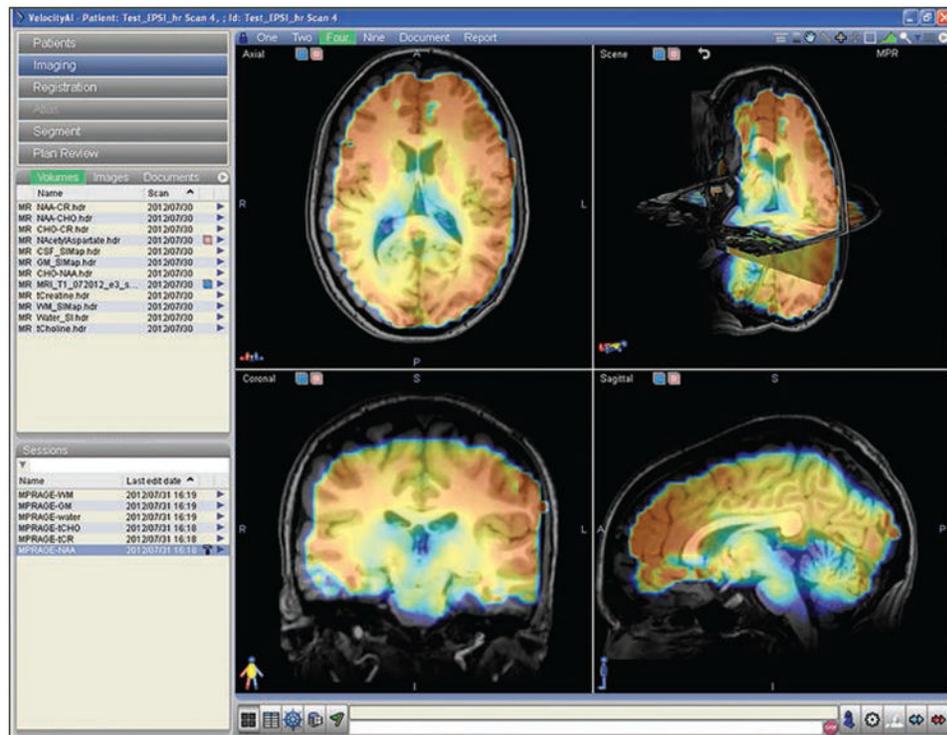
**Fig. 1.**
Display of *N*-acetyl aspartate (NAA) 3D map fused with T1-weighted magnetization-prepared rapid gradient-echo images in Velocity AI imaging platform. MR spectroscopic image was obtained with TR/TE, 1710/17 and inversion time, 198 ms with nominal voxel size of $4.4 \times 4.4 \times 5.6$ mm (0.108 mL). NAA concentration in arbitrary units was calculated by its ratio over brain-water signal from same ROI, with adjustment for brain-water content determined from FLASH sequence.
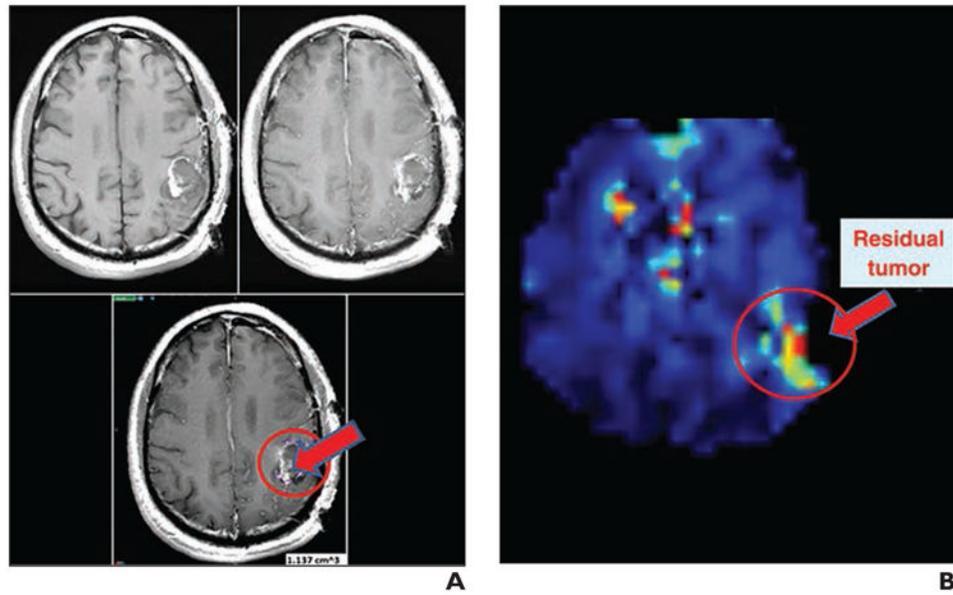
**Fig. 2.**
Choline (Cho)/*N*-acetyl aspartate (NAA) ratio map of MR spectrographic image reveals residual tumor (*arrow*) better than MRI alone in glioblastoma patients after surgical resection.

**A**, To estimate residual glioblastomas, T1-weighted image (top left) was subtracted from contrast-enhanced T1-weighted image (top right). Difference map (bottom) shows residual tumors marked in purple inside of red circle using Velocity AI program (Velocity Medical Solution).

**B**, Cho-to-NAA ratio map was calculated using Metabolic Imaging Data Analysis System (University of Miami) and displayed using Velocity AI. Residual tumors based on elevated Cho-to-NAA ratio are indicated by red arrow inside of red circle. Some motion artifacts are shown in lesions of ventricle and sinus in top and center area.
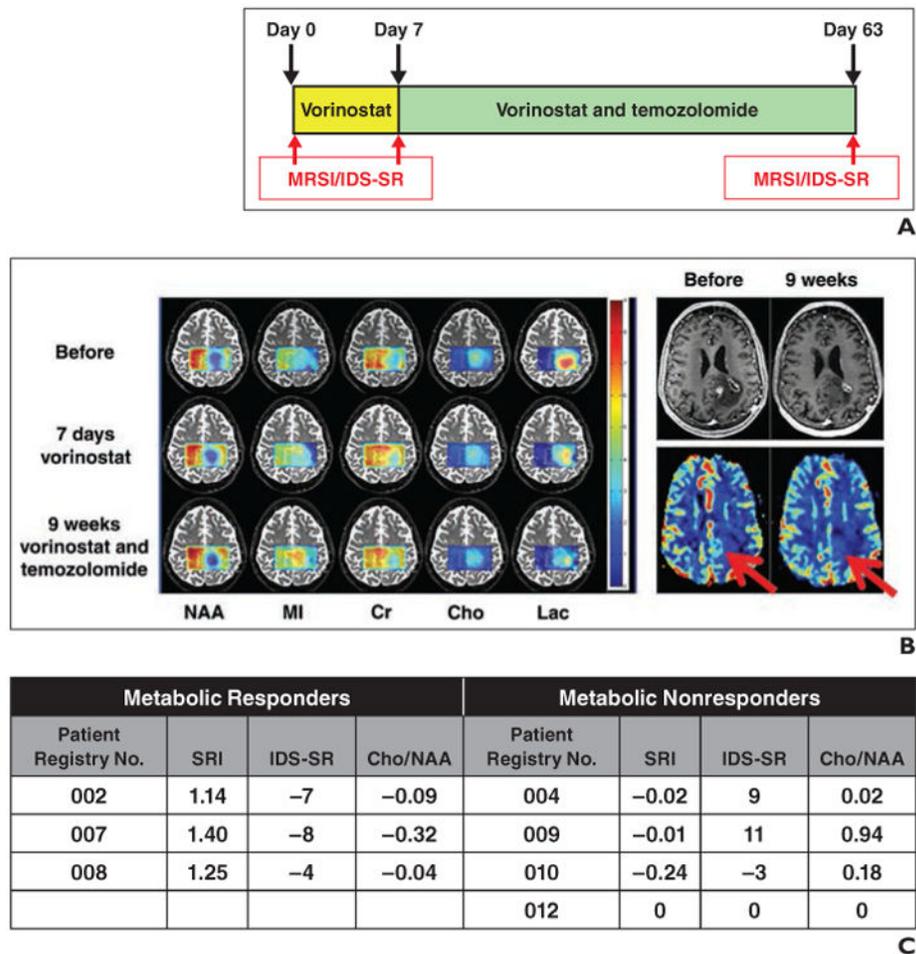
**Fig. 3.**

Treatment with vorinostat and temozolomide.

**A,** Bar chart shows scheme of treatment and imaging session schedule. MRSI= MR spectroscopy imaging, IDS-SR = Inventory of Depressive Symptoms-Self Report.

**B,** Map of various metabolites derived from stimulated-echo acquisition mode–based 2D chemical-shift imaging in 71-year-old man before, after 7 days of treatment with vorinostat alone, and after 63 days of vorinostat and temozolomide treatment. Increased *N*-acetyl aspartate (NAA), creatine (Cr), and myoinositol (MI) and decreased lactate (Lac) suggest restoration of normal brain tissuelike metabolism in vorinostat-treated tumor. Contrast-enhanced T1-weighted MR images (*top*) and relative cerebral blood volume maps (*bottom*) in this patient before and after 63 days of treatment are shown on right. Arrows indicate hyperperfusion area in relative cerebral blood volume map with suspected viable tumors that are not seen on scan taken at 9 weeks. Cho = choline.

**C,** Chart shows spectroscopic restoration index (SRI), IDS-SR scores, and Cho-to-NAA ratio at day 7 compared with day 0 for seven patients who enrolled in Quick Trial of vorinostat and temozolomide. Those patients who completed study were all listed here. Negative values indicate improvement in IDS-SR scores, and positive values indicate worsening.
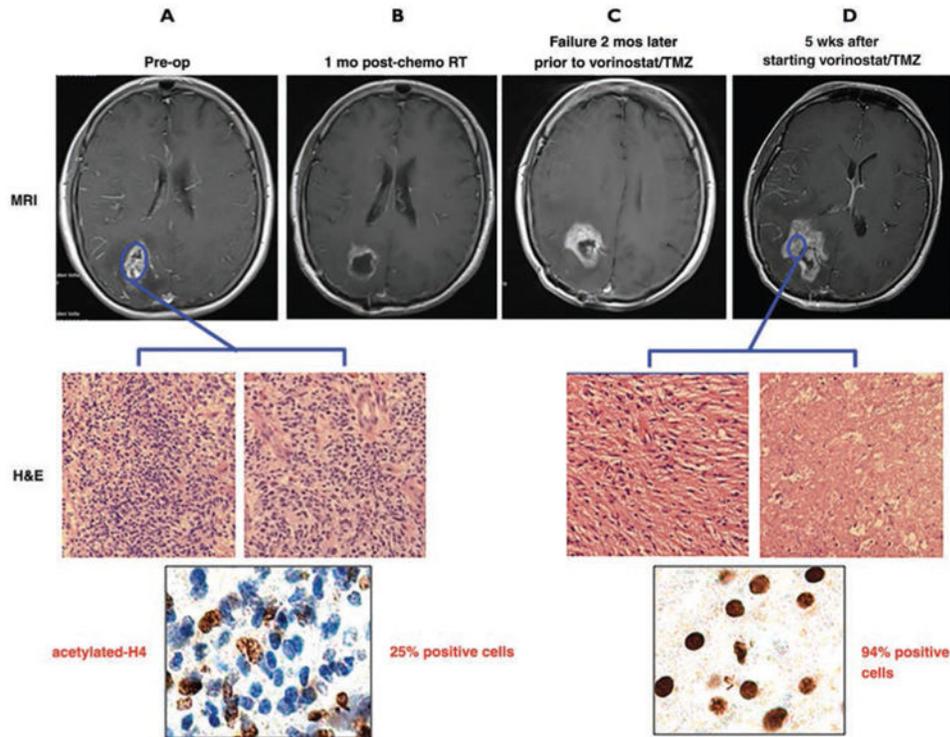
**Fig. 4.**
55-year-old woman who enrolled in vorinostat and temozolomide (TMZ) trial who showed metabolic responder MR spectroscopic imaging (MRSI) results. **A–D,** Before surgery, T1-weighted MRI showed typical features of glioblastomas and matching pathology results (**A**). Patient was enrolled in study at 3 months after radiation therapy (RT) and TMZ treatment because follow-up contrast-enhanced T1-weighted MRI (**C**) showed increased enhancing area compared that of 1 month after RT and TMZ treatment (**B**). Although her MRSI data showed patient as metabolic responder, she was removed from our trial at week 5 due to worsening contrast-enhanced T1-weighted MRI (**D**). One week later, enhancing lesion was biopsied and H and E stained to confirm well-differentiated tumors and necrotic tissues (**D**). In addition, immunohistochemical analysis using antibody against acetylated histone H4 was performed to confirm activity of histone deacetylase inhibitor.